Lawrence Berkeley National Laboratory

Title
Beam Energy Scaling on Ion-Induced Electron Yield from K+ Impact on Stainless Steel

Permalink
https://escholarship.org/uc/item/26p163ww

Authors
Kireeff Covo, Michel
Molvik, Arthur
Friedman, Alex
et al.

Publication Date
2006

Peer reviewed

Beam Energy Scaling of Ion-Induced Electron Yield from K⁺ Impact on Stainless Steel

Michel Kireeff Covo

Lawrence Livermore National Laboratory, Heavy-Ion Fusion Virtual National
Laboratory, Livermore, California 94550, USA and

University of California at Berkeley, 4155 Etcheverry Hall, MC 1730, Berkeley, CA
94720, USA

Arthur Molvik, Alex Friedman, Glen Westenskow, John J. Barnard, Ronald Cohen,
David Grote, and Steven M. Lund

Lawrence Livermore National Laboratory, Heavy-Ion Fusion Virtual National
Laboratory, Livermore, California 94550, USA

Peter Seidl, Joe W. Kwan, Grant Logan, David Baca, Frank Bieniosek, Christine M.
Celata, and Jean-Luc Vay

Ernest Orlando Lawrence Berkeley National Laboratory, Heavy-Ion Fusion Virtual
National Laboratory, 1 Cyclotron Road, Berkeley, California 94720, USA

Jasmina L. Vujic

University of California at Berkeley, 4155 Etcheverry Hall, MC 1730, Berkeley, CA
94720, USA

Electron clouds limit the performance of many major accelerators. Significant quantities of electrons result when halo ions are lost to beam tubes, generating gas which can be ionized and ion-induced electrons that can multiply and accumulate, causing degradation or loss of the ion beam. In order to understand the physical mechanisms of ion-induced electron production, experiments studied the impact of 50 to 400 keV K⁺ ions on stainless steel surfaces near grazing incidence, using the 500 kilovolts Ion Source Test Stand (STS-500) at LLNL. The experimental electron yield scales with the

electronic component (dE_e/dx) of the stopping power. A theoretical model is developed, using TRIM code to evaluate dE_e/dx at several depths in the target, to estimate the electron yield, which is compared with the experimental results.

I. INTRODUCTION

Ions hitting the walls of accelerators or storage rings desorb gas [1,15] and electrons [12,13,15]. The gas can move into the path of the beam and be ionized. The electrons may bounce back and forth between the walls in a resonant motion, with a very fast pressure rise due to electron-stimulated gas desorption. If enough electrons and gas accumulate, they will cause degradation or loss of the beam. This is the electron cloud effect, a recognized problem in positively-charged-particle accelerator rings and a potential design constraint for the low energy (1 MeV) region of intense beam ion linacs for high energy density physics and heavy ion fusion [2].

One of the first observations of beam-induced multipacting effects with a characteristic pressure rise was in the Intersecting Storage Rings (ISR) at CERN [3]. Proton halo from the Spallation Neutron Source (SNS), under construction at ORNL, can hit surfaces, mainly the collimators, and is expected to generate electrons and produce instabilities [4]. In order to measure beam scraping effects on secondary electron production in conditions similar to those of the SNS collimators, the ion beam from the Alternating Gradient Synchrotron (AGS) booster at BNL was intentionally steered into the electrostatic inflector [5].

Major issues for electron cloud threshold in hadron colliders, such as the Relativistic Heavy Ion Collider (RHIC) at BNL and Large Hadron Collider (LHC) at CERN, include the secondary electron production and survival rate in the bunch gap [6]. The High Current Experiment (HCX) at LBNL is being used to identify and quantify sources of electrons and validate three-dimensional self-consistent WARP simulations of electron cloud effects [7,8].

Currently, methods for mitigation including coating with NEG and TiN [9], cleaning and outgassing procedures [10] and solenoidal magnetic fields [11] are being used in major accelerators. Newly proposed methods like serrated plates [12], annular ridges [13,14] and bead blasted surfaces [15] are under investigation; these aim to reduce

grazing-incidence ion collisions, decreasing electron emission yield and minimizing electron cloud effects.

The main goal of the present work is to check our understanding of the mechanism of ion-stimulated electron production near grazing incidence. For that we acquired data with the Gas-Electron Source Diagnostic (GESD) [15] using the STS 500 facility [35] with K^+ ions hitting a stainless steel target. The energy ranged from 50 keV to 400 keV, represented in Fig. 1 with gray color, where nuclear stopping power transitions to electronic stopping power predominance.
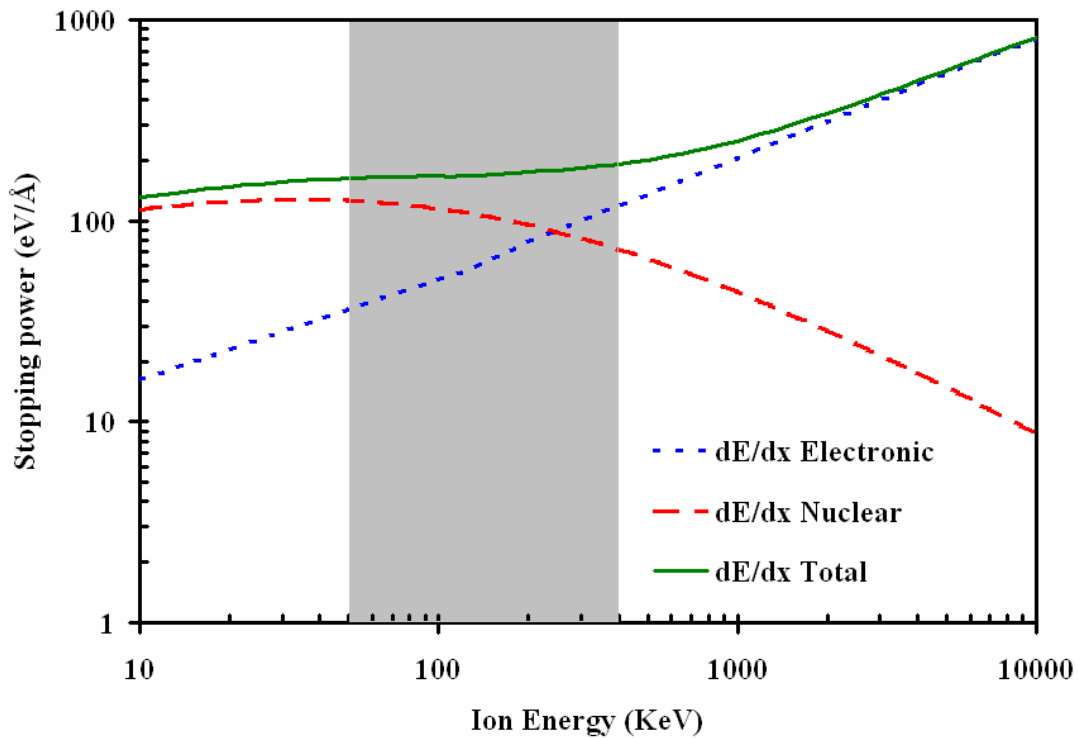

FIG. 1. (Color) Stopping power for K^+ ions hitting stainless steel target, from TRIM 2003 calculations.

Section II will discuss theory and methods of ion-induced electrons generation. The main mechanism will utilize the kinetic energy from the incident ion to excite the electron, transport it to the surface and cross the surface barrier. A model based in Sternglass theory will be explained. Section III will simulate the dynamics of K^+ ion collisions with stainless steel target near grazing incidence using TRIM (the Transport of Ions in Matter [16]) program. The generation of electrons and transport to the surface will be estimated, giving the ion-induced electron yield. Section IV will describe the GESD

experiment on the 500 kilovolts Ion Source Test Stand (STS-500) facility and compare some experimental data with the theoretical results. Section V will discuss the results and possible reasons for small discrepancies observed. Finally, section VI will summarize our conclusions.

II. THEORY OF ION-INDUCED ELECTRONS

There are two distinct mechanisms for releasing electrons from a solid under bombardment: potential electron emission and kinetic electron emission.

A. Potential Electron Emission (PEE)

PEE uses the energy released upon the neutralization of an ion. The incident ion can liberate electrons from the metal, only if the ground-state recombination energy of the ion exceeds twice the work function of the target. PEE yields are reasonably constant for ion velocities under 5×10^5 m/s, corresponding to a K ion with energy of 51.22 keV, and steeply decrease at higher velocities [17]. The K^+ ion used in the present work has the initial ionization energy of 4.341 eV [18], which is smaller than two times the work function of stainless steel ($\varphi \cong 4.4$ eV), so the projectile does not have enough potential energy to cause electron emission by this mechanism before entering the solid. However, once the ion is in the material, it becomes charge-equilibrated after interacting with the top layers, as calculated below. The ionized or excited ion could have enough potential energy to enable PEE.

The Thomas-Fermi model predicts the average velocity of the bound electron:

$$V_{e,bound} \cong 2.2 \times 10^6 \left(Z_p\right)^{2/3} \text{ [m/s].} \tag{1}$$

Assuming that all the electrons of the ion with orbital velocity less than the projectile velocity are stripped [19], a rough estimate of the equilibrium charge inside the solid is:

$$Z_{eq} = \left(1 - e^{-\frac{V_p}{V_{e,bound}}}\right)^{1/2} Z_p. \tag{2}$$

From equation (2), for a K^+ ion with energy of 50 to 400 keV, the equilibrium charge is in the range of 3 to 6. These values are too high if compared with experimental

data from 150 keV K in Mg foil [20], which gives 24% of K^{0+}, 55% of K^{1+}, 19% of K^{2+} and only 1.9% of K^{3+}.

The electrons that are stripped off will have a forward peaked distribution with an average energy in the laboratory frame of:

$$E_{eq} = \frac{m_e}{M} E_{ion},$$

(3)

where m_e is the electron mass, M is the ion mass and E_{ion} is the ion energy. This energy is called loss-peak-energy [21] and corresponds to the kinetic energy of a free electron running at the ion velocity. The loss-peak-energy for a 50 to 400 keV K^+ ion is 0.69 to 5.54 eV.

The potential energy obtained can be released if the stripped ion is backscattered and neutralized or if it stops in the material (thereby exciting atoms, which can produce decay by Auger processes). A simple model [22,23] predicts a maximum escape depth for electrons ($\delta \sim 2nm$), so the Auger electrons will have a chance of escaping only if produced inside that layer.

The semiempirical yield dependence [24] for the potential energy from the backscattered ions is:

$$\gamma_P = \frac{0.2}{\varepsilon_F}\left(0.8W_q - 2\varphi\right),$$

(4)

where ε_F is the Fermi energy (≈ 11.1 eV for iron), φ is the work function (≈ 4.4 eV for stainless steel) and W_q is the potential energy of the stripped K ion (≈ 35.97 for K^{+2}). This gives $\gamma_P = 0.36$ electrons ejected for PEE by K^{+2}.

If we assume that, for the energy range of this work, 20% of the ions will have this charge state and only they will produce electrons by PEE, γ_P decreases to 0.072.

The backscattered-ion PEE yield contribution will increase with the increasing number of backscattered ions (or angle). TRIM simulations summarized in table I (discussed below) show up to 70% backscattering, giving γ_P from backscattering of 0.0504.

In addition, the backscattered ions can also emerge accompanied by electrons captured in the continuum state, called convoy electrons [25].

5

Table I also shows a large amount of sputtered material, which will be ionized inside the metal and can contribute to the PEE. The charge distribution of the sputtered ions will be a function of their energy. Assuming an average sputtering yield of 30 and γ_P ≈ 0.072 for Fe, Ni and Cr sputtered, γ_P from sputtering will be ≈ 2.16.

The total PEE contribution from backscattered and sputtered ions will be ≈ 2.21. The semiempirical formula does not take into account the projectile velocity and therefore gives an upper limit.

B. Kinetic Electron Emission (KEE)

KEE, the other mechanism for releasing electrons, occurs at the expense of the kinetic energy of the projectile. At higher velocities most of the ejected electrons are generated in direct binary collisions of the ions with the valence electrons or with target atoms. The process involves normally three steps: the excitation of the electron, its transport to the surface, and its escape through the surface barrier. The KEE will happen only if the projectile velocity is above a certain threshold [26].

Using the free electron gas model, the maximum energy transferred in a binary interaction with a light projectile is:

$$T_M = 2m_e v(v + v_F), \qquad (5)$$

where m_e is the mass of the electron, v is the velocity of the ion and v_F is the Fermi velocity ($v_F \approx 1.98 x 10^6$ m/s for iron). This gives a maximum energy transferred of 13.9 to 53.6 eV for 50 to 400 keV K^+ ion interacting with iron, respectively.

Threshold velocities for the KEE are obtained by setting T_M equal to the work function of the material. For stainless steel, the threshold velocity will be approximately $1.79 x 10^5$ m/s, corresponding to a 6.58 keV K^+ ion. Given the possibilities that the valence electrons can exchange momentum with the lattice during the excitation or that the electron-electron interaction is more efficient for heavy ions as the electron clouds are compressed during the collision, the maximum energy transferred will be greater than the value shown above and consequently the threshold velocity will be below that range [27].

6

From this discussion and the experimental data shown in section IV, it can be concluded that the main electron emission mechanism will be KEE for the present ion energy range.

An ion entering a solid will lose energy to the medium. The energy loss from the projectile per unit path length is known as stopping power, which has two components, the nuclear and the electronic, shown in Fig. 1. The nuclear stopping power is caused by elastic collisions with the nuclei of the target material; the electronic stopping power is produced by inelastic collisions with the electrons.

Sternglass [28] developed a model that considered the energy lost by incident ions in distant and close collisions, producing slow and fast secondaries, respectively. The fast secondaries will slow down and produce more secondaries. He ended up with a very simple expression with the ion induced electron emission yield γ_e proportional to the electronic stopping power.

Schou [29] demonstrated the proportionality of γ_e and the energy deposited on the surface by an incident ion using electron transport equations. For the KEE, neglecting surface roughness and assuming that the energy transferred to the electrons is greater than the ionization plus the work function of the material, the number of electrons excited by projectile above the vacuum level in the interval x to x +dx is given by:

$$\gamma_e = \int P \frac{E}{J} dx ,$$

(6)

where E is the energy transmitted to the electrons, P is the fraction of electrons moving towards the surface and J is the average energy to generate an electron. E will be the electronic stopping power times the path length L, which is equal to maximum escape depth (δ) times $cos(\theta)^{-1}$, where θ is the ion angle from the surface normal.

Assuming the electronic stopping to be almost constant, γ_e will be:

$$\gamma_e = \frac{\delta}{J} \frac{P}{\cos(\theta)} \left(\frac{dE}{dx} \right)_e = \Lambda_M \frac{P}{\cos(\theta)} \left(\frac{dE}{dx} \right)_e ,$$

(7)

where Λ_M is a material parameter called "specific yield".

Rothard [30] confirmed the proportionality of electron emission to the electronic stopping power for a wide range of projectile velocities (15 keV/u $\leq$ E$_P$/M$_P$ $\leq$ 16 MeV/u) and projectile nuclear charges Z$_P$ (1 $\leq$ Z$_P$ $\leq$ 92).

If γ_e is tabulated for proton projectile, a constant C can be introduced to account for variations of the ion species, giving:

$$\gamma_e = C\Lambda_M \frac{P}{\cos(\theta)} \left(\frac{dE}{dx} \right)_e .$$

(8)

Experimental data for γ_e has been evaluated, finding C to be approximately 0.32 for heavy ions [30,31].

III. TRIM SIMULATION

TRIM is a program that calculates the stopping and range of ions into matter using a quantum mechanical treatment of ion-atom Coulomb collisions [16]. It considers the velocity dependent charge state of the ion and the long range screening interactions, which can create electron excitations and plasmons within the target. The target can be made of up to eight layers of compounds and elements. TRIM follows each ion collision and all target atom cascades, providing details of ion distribution, target damage, sputtering, ionization, and phonon production.

Table I was obtained for 10,000 K ions hitting stainless steel, using the TRIM program with the stopping power version SRIM-2003. The simulation shows that 40-70% of the ions are backscattered and can cross the electron escape layer twice, losing energy, producing recoils and changing charge state and direction.

K+ ion Energy (KeV)	Depth (Å)		Backscattering Yield		Sputtering Yield	
	82°	88°	82°	88°	82°	88°
50	108 ± 76	104 ± 73	0.51	0.70	27.24	19.14
130	246 ± 165	232 ± 155	0.49	0.70	31.38	24.6
202	359 ± 234	350 ± 227	0.48	0.69	31.37	26.02
305	504 ± 329	480 ± 312	0.46	0.69	29.81	28.51
393	632 ± 402	592 ± 377	0.45	0.68	27.78	29.02
972	515 ± 258	1132 ± 719	0.40	0.66	18.56	30.04

Table I. TRIM 2003 simulation of K^+ ion hitting stainless steel at different energies and angles from normal.

KEE has two components, one is primarily related to the electronic stopping power from the projectile and the other is related to nuclear stopping power, which will generate recoils that can ionize the medium [32], giving a contribution that is not considered in equation (8). In addition, ions near grazing incidence will travel more along the first few atomic layers, which correspond to the electron escape layer, losing energy, changing direction and some of them being backscattered (the term "backscatter" is defined in TRIM program and in this paper as scattering back out of a surface). Consequently there are no defined angles and energy losses for the ions and recoils. The TRIM program can overcome some of these limitations providing the ion and recoil energy loss to target electrons as a function of target depth.

Equation (8) can be rewritten as

$$\gamma_e = C\frac{P}{J}\left[\frac{\delta}{\cos(\theta)}\left(\frac{dE}{dx}\right)_e\right] = C\frac{P}{J}\sum_{x=0}^{\delta} E_{TRIM}(x),$$ **(9)**

where $E_{TRIM}(x)$ is the total ionization data provided by TRIM code as a function of target depth x and δ is the depth of the electron escape layer.

Fig. 2 shows an example of the energy loss obtained using TRIM program. It discriminates the ions and recoils energy loss source from 50 keV K^+ ions hitting stainless steel target at 82 degrees from normal. The energy loss by ions is bigger near the

9

surface, reaches a maximum after few angstroms and becomes smaller than the loss by recoils after 41 Å of target depth.
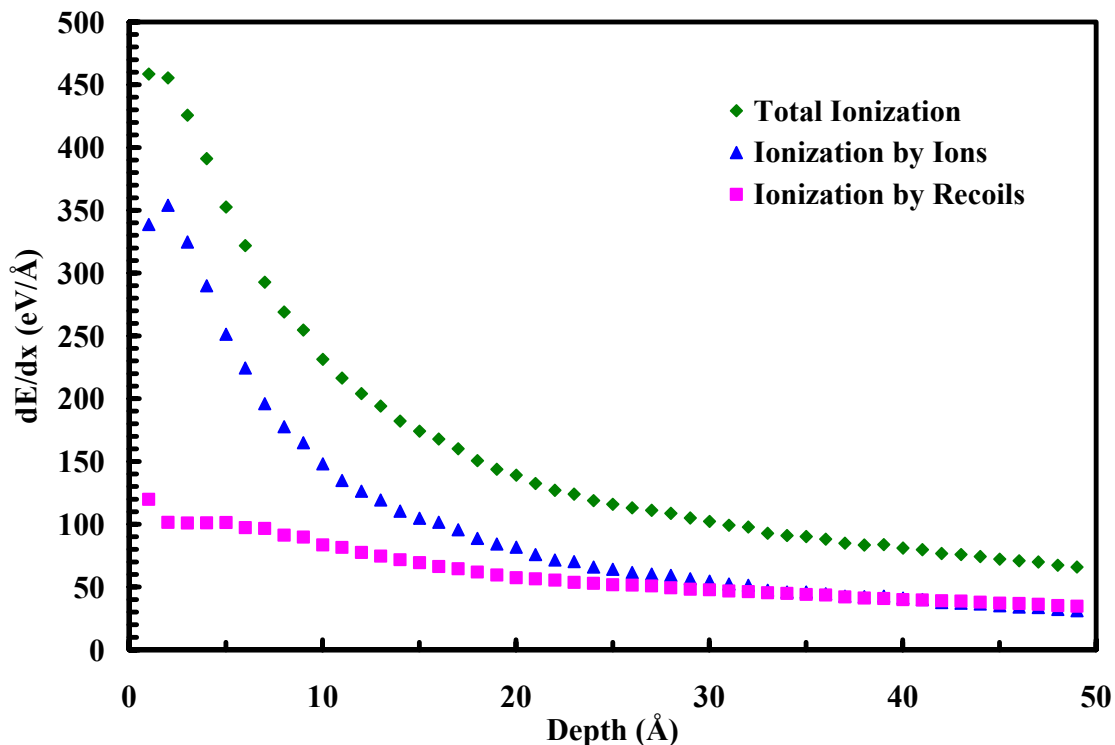

FIG. 2. (Color) Energy loss of 50 keV K ion at 82 degrees from normal to the target electrons by ions and recoils.

Assuming that the ion-induced electrons have enough energy to cross the surface barrier and are proportional to the released ionization energy, the number of electrons generated as a function of target depth can be obtained by dividing the ionization energy released at that depth by the average energy that generated the electron, i.e., $N_0(x) = E_{SRIM}(x)/J$. If this amount is deposited along the distance traveled into the stainless steel target towards the surface, using a first order decay law typical of radiation transport through matter, the result is:

$$\gamma_e = CP \sum_{x=0}^{\delta} \frac{E_{TRIM}(x)}{J} e^{\left(\frac{-x}{L}\right)} = CP \sum_{x=0}^{\delta} N_0(x) e^{\left(\frac{-x}{L}\right)}, \tag{10}$$

where x is the distance to the surface and L is the mean attenuation length.

The mean attenuation lengths for electrons in metals, averaged over the ion-induced electron spectrum, are in the range of 5 to 15Å [33].

10

Fig. 4(a) was obtained by assuming $P \approx 0.5$, $J \approx 25\text{eV}$ [34], $\delta = 20\text{Å}$, $C \approx 0.32$ and $L = 10\text{ Å}$ as typical values of a heavy-ion hitting a metal, and $E_{TRIM}(x)$ given by 10,000 K^+ hitting stainless steel for angles between 82 and 89 degrees in the energy range from 50 to 400 keV.

IV. EXPERIMENT

In order to measure the electron yield that would be produced by halo particle impacts near grazing incidence, the GESD was placed at the end of a 500 kilovolts ion source test stand (STS-500) [35], which can generate a 1 A, 17 μs pulse of 500 keV K^+ ions every few seconds.

The GESD, shown in Fig. 3, consists of several electrodes that can be independently biased. It is designed to measure gas desorption and ion-induced electron emission from heavy-ion beams impacting a surface near grazing incidence. The design and commissioning of the GESD are described in greater detail in Ref. [15]. The beam current passing through a small aperture (0.1 x 2.0 cm for these experiments) hits the stainless steel target electrode. The target is treated using the LBNL ultrahigh vacuum cleaning procedures [36] and is adjustable between angles of incidence of 82 to 89 degrees from normal to the surface. Between the aperture and the target there is a suppressor electrode to prevent electrons from entering or leaving the GESD. At the end of the target a catcher electrode is placed to capture most of the reflected ions. Around the target there is a grid and under the target a Faraday cup (FC) is positioned.

The electron emission current is measured when the target is positioned to be struck by the apertured beam at an angle between 82 and 89 degrees, biasing the grid to +150 V, the electron suppressor to -200 V, the catcher to -25 V and the target at -40 V. The apertured beam current entering the GESD can be measured by centering the Faraday cup in front of the aperture, biasing the Faraday cup to -40 V, and the suppressor to -200 V. The electron yield (number of electrons produced by each ion) is the ratio of the electron emission current from the target to the apertured beam current going into GESD.
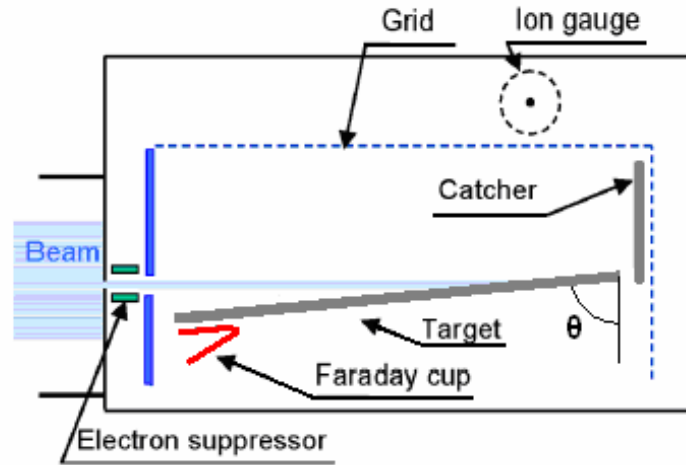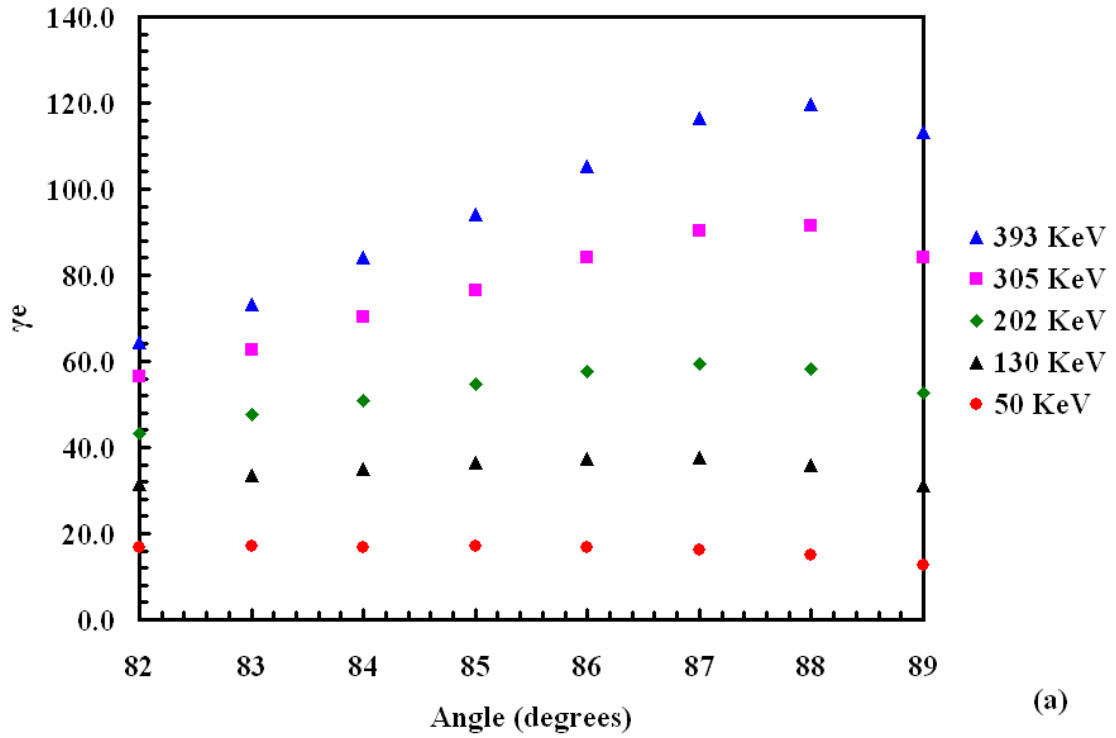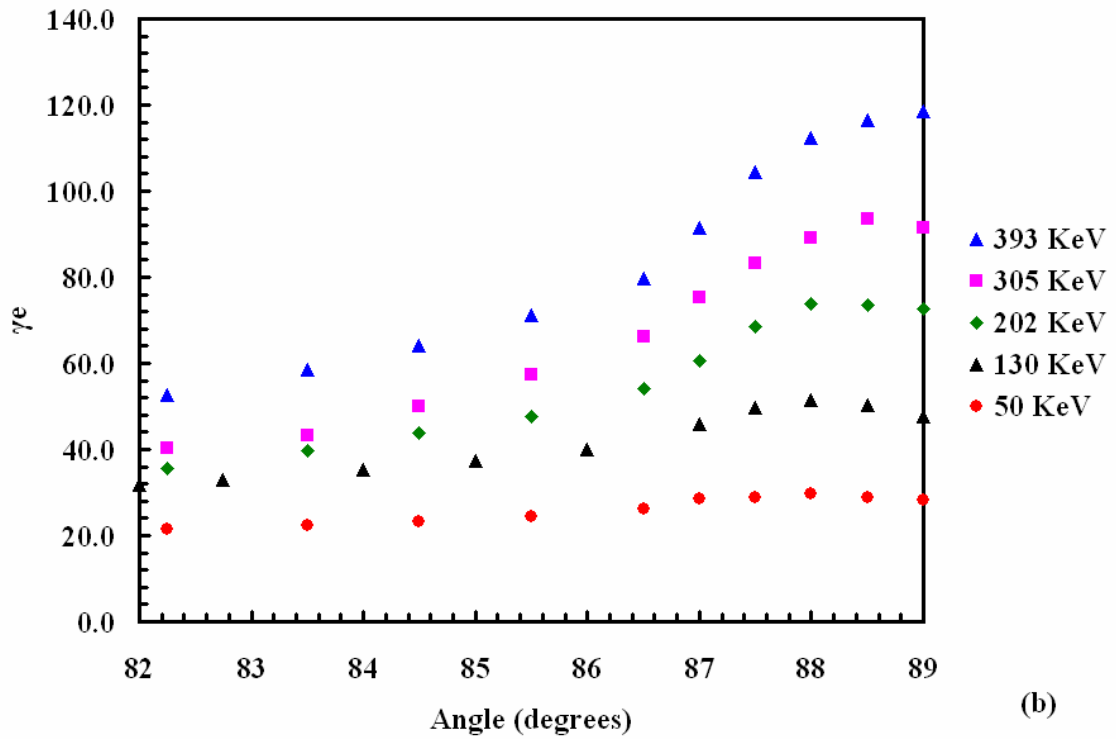
FIG. 3. Gas-Electron Source Diagnostic (GESD).

Fig. 4(b) shows GESD measurements done with the STS-500. The K^+ ions hit the stainless steel target with energy up to 400 keV. The angles measured were between 82 to 89 degrees from normal incidence.

FIG. 4. (Color) Ion-induced Electron Emission. (a) Theoretical γ_e for K^+ ions with different energies hitting stainless steel target obtained from equation (10). (b)

Experimental γ_e for K$^+$ ions with different energies hitting stainless steel target obtained using GESD at STS-500.

Fig. 5 compares the experimental electron yield at 88 degrees from the HCX facility with data obtained at STS-500 [37].
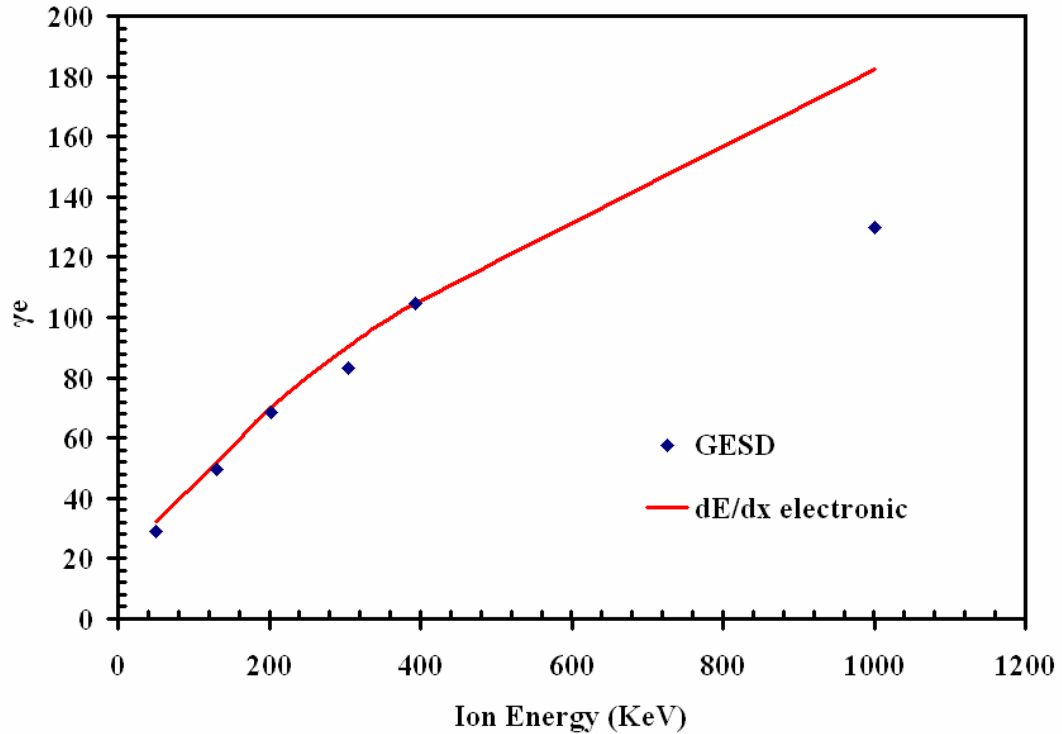

FIG. 5. Electron Yield obtained with Gas-Electron Source Diagnostic at 88 degrees compared with the electronic stopping power normalized to 392.8 keV.

V. DISCUSSION

Fig. 5 shows that the electron yield at 980 keV did not scale with the electronic stopping power, revealing a 40% difference. The model developed here using the TRIM program did not explain the difference. The escape depth of electrons inside a solid is only a few atomic layers [38], which enhances the effects of surface conditions. Adsorbed and desorbed gases have different electron excitation probabilities and can change the surface barrier. The experiments were performed one year apart, leading to concern that the difference observed is due to surface contamination or due to electron creation and transport issues that were assumed alike in the energy interval.

14

It can be seen in Fig. 4(b) that for lower energies there is a weaker variation of γ_e with angle than $cos(\theta)^{-1}$. This energy angle dependence was noticed previously and attributed to three possible factors: scattering and slowing down of the projectile in the region of greater electron escape probability, influence of recoiling target atoms, and anisotropy in the source of excited electrons [39].

The model developed using the TRIM program simulates the first two possibilities, and the results are plotted in Fig. 4(a). It confirms that for lower energies the ion range decreases and an almost constant fraction of ions and recoils energies will be lost within the electron escape zone, regardless of the angle.

At higher energies the nuclear stopping power is small, so the ions cross the electron escape zone with a defined angle and energy loss, concurrent with the decreasing amount of backscattered ions, giving a better fitting of γ_e with angle as predicted in equation (8) [12,15].

Another feature from Fig. 4(b), not observed in Fig. 4(a), was a subtle change of slope at 87 degrees which may be attributed to the anisotropy in the source of excited electrons concurrent with the enhancement of the interaction of the surface with the projectile near 90 degrees.

TRIM considers the target amorphous and neglects material structure and surface roughness. The theoretical electron yield, shown in Fig. 4(a), is sensitive to the assumptions made at the end of section III. Not all the electrons going towards the surface will be transmitted, and some of them will collide as they travel and generate a cascade, which can propagate. The energy dependence of the averaged mean attenuation length and the average energy to generate an electron should also be considered when comparing experiment and model over a large energy range.

VI. CONCLUSIONS

K^+ ions hitting stainless steel near grazing incidence with energies in the range of 50 to 400 keV will produce electrons mainly by KEE, yielding experimental emission coefficients of 21 to 119 compared with theoretical emission coefficient corrected for the PEE contribution of 15 to 122. The ions will be stripped and change charge state as they lose energy inside the electron escape layer. Therefore, the electronic stopping power will

15

not remain constant [12,40]. Backscattered ions that can cross the electron escape layer twice and recoil ions will also be produced, making it difficult to calculate the total energy released to the electrons.

A model to overcome these difficulties and estimate the ion-induced electron yield by the KEE mechanism for ions hitting a target near grazing incidence is proposed. The model uses the TRIM code to calculate dE_e/dx as function of target depth and infers the number of electrons produced, which will be damped to account for their transport to the surface. The model disregards target material structure, cascade of electrons, or any anisotropy of production of electrons.

Even without taking into account more complex physics, the yield calculated resembles the experimental data obtained, but does not capture all the details of the experimental data. The experimental electron yield scales with dE_e/dx over the ion energy range of 50 to 400 keV, extending the results reported in Ref. [30].

ACKNOWLEDGEMENTS

[1] E. Mahner, J. Hansen, D. Küchler, M. Malabaila, and M. Taborelli, Phys. Rev. ST AB **8**, 053201 (2005).

[2] *Proceedings of the eCloud'04 Workshop*, *Napa Valley*, *California*, *2004*, http://icfa-ecloud04.web.cern.ch/icfa-ecloud04/.

[3] O. Gröbner, Proceeedings of the 10th International Accelerator Conference,
Serpukhov, 1977, p. 277.

[4] W. T. Weng, J. Alessi, J. Beebe-Wang, M. Blaskiewicz, L. Blumberg, M.
Brennan, C. Gardner, Y. Y. Lee, A.U. Luccio, H. Ludewig, D. Maletic, D. Raparia,
A. Ruggiero, and S. Y. Zhang, IEEE Particle Accelerator Conference, Vancouver, 1999,
p. 970.

[5] S. Y. Zhang, IEEE Particle Accelerator Conference, New York, 1999, 3297.

[6] M. A. Furman, LBNL Report No. 50765, 2002.

[7] R. H. Cohen, A. Friedman, S. M. Lund, A. W. Molvik, T. Azevedo, J.-L. Vay, P.
Stoltz, and S. Veitzer, Nucl. Instrum. Methods Phys. Res. A **544**, 210 (2005).

[8] R. H. Cohen, A. Friedman, S. M. Lund, A. W. Molvik, E. P. Lee, T. Azevedo, J.-L.
Vay, P. Stoltz, and S. Veitzer, Phys. Rev. ST Accel. Beams **7**, 124201 (2004).

[9] P. He, H. C. Hseuh, M. Mapes, R. Todd, and D. Weiss, in *Proceedings of IEEE*
Particle Accelerator Conference, Chicago IL, 2001, p. 2159.

[10] J. R. Noonan, J. Gagliano, G. A. Goeppner, R. A. Rosenberg and D. R. Walters, in
Proceedings of IEEE Particle Accelerator Conference, Vancouver, Canada, 1997, p.
3552.

[11] L.Wang, S. Kurokawa, H. Fukuma, S. S. Win, and A.Chao, in *Proceedings of the*
eCloud'04 Workshop, Napa Valley, California, 2004, http://icfa-
ecloud04.web.cern.ch/icfa-ecloud04/.

[12] P. Thieberger, A. L. Hanson, D. B. Steski, V. Zajic, S. Y. Zhang, and H. Ludewig,
Phys. Rev. A **61**, 042901 (2000).

[13] P. Thieberger, W. Fischer, H. Hseuh, V. Ptitsyn, L. P. Snydstrup, D. Trbojevic, and S. Y. Zhang, Phys. Rev. ST Accel. Beams **7**, 093201 (2004).

[14] S. Y. Zhang, H. C. Hseuh, P. Thieberger, and D. Trbojevic, Phys. Rev. ST Accel. Beams **8**, 123201 (2005).

[15] A. W. Molvik, M. Kireeff Covo, F. M. Bieniosek, L. Prost, P. Seidl, D. Baca, A. Coorey, and A. Sakumi, Phys. Rev. ST AB **7**, 093202 (2004).

[16] J. F. Ziegler, http://www.srim.org/.

[17] E. V. Alonso, R. A. Baragiola, J. Ferron, M. M. Jakas and A. Olivia-Florio, Phys. Rev. B **22**, 80 (1980).

[18] R. J. Borg and G. J. Dienes, *The Physical Chemistry of Solids* (Academic Press, San Diego, 1992).

[19] N. Bohr, Phys. Rev. **59**, 270 (1941).

[20] A. B. Wittkower and H. D. Betz, Atom. Data **5**, 113 (1973).

[21] H. Kudo, K. Shima, S. Seki, K. Takita, K. Masuda, K. Murakami and T. Ippshi, Phys. Rev. B **38**, 44 (1988).

[22] H. Bruining, *Physics and Applications of Secondary Electron Emission* (Pergamon Press, London, 1954).

[23] J. L. H. Jonker, Philips Research Report 7, 1 (1952).

[24] L. M. Kishinevsky, Rad. Eff. **19**, 23 (1973).

[25] A. Koyama, Y. Sasa, H. Ishikawa, A. Misu, K. Ishii, T. Iitaka, Y. H. Ohtsuki and M. Uda, Phys. Rev. Let. **65**, 3156 (1990).

[26] E. V. Alonso, M. A. Alurralde and R. A. Baragiola, Surf. Science **166**, L155 (1986).

[27] R. A. Baragiola, E. V. Alonso, J. Ferron and A. Oliva-Florio, Surface Sci. **90**, 240 (1979).

[28] E. J. Sternglass, Phys. Rev. **108**, 1 (1957).

[29] J. Schou, Phys. Rev. B **22**, 2141 (1980).

[30] H. Rothard, K. Kroneberger, A. Clouvas, E. Veje, P. Lorenzen, N. Keller, J. Kemmler, W. Meckbach and K.–O. Groeneveld, Phys. Rev. A **41**, 2521 (1990).

[31] P. H. Stoltz, M. A. Furman, J.-L. Vay, A. W. Molvik and R. H. Cohen, Phys. Rev. ST AB **6**, 054701 (2003).

[32] G. Holmén, B. Svensson, J. Schou, and P. Sigmund, Phys. Rev. B **20**, 2247 (1979).

[33] R. A. Baragiola, Nucl. Inst. and Meth. B **78**, 223 (1993).

[34] P. H. Stoltz, S. Veitzer, R. Cohen, A. W. Molvik and J.-L. Vay, Phys. Rev. ST AB **7**, 103201 (2004).

[35] J. W. Kwan, D. Baca, E. Henestroza, J. Kapica, F. M. Bieniosek, W. L. Waldron, J. - L. Vay, S. Yu, G. A. Westenskow, D. P. Grote, E. Halaxa, I. Haber, and L. Grisham, Nucl. Instrum. Methods Phys. Res. A **544**, 134 (2005).

[36] K. Kennedy, LBNL Report No. LSME-323, 1990.

[37] M. Kireeff Covo et al., in *Proceedings of IEEE Particle Accelerator Conference, Knoxville TN, 2005*, p. 2287.

[38] H. J. Fitting, H. Glaefeke, and W. Wild, Surf. Sci. **75**, 267 (1978).

[39] J. Ferrón, E. V. Alonso, R. A. Baragiola and A. Oliva-Florio, Phys. Rev. B **24**, 4412 (1981).

[40] G. Lakits, A. Arnau and H. Winter, Phys. Rev. B **42**, 15 (1990).